Analytica Chimica Acta 1063 (2019) 152–158

Contents lists available at ScienceDirect

Analytica Chimica Acta

journal homepage: www.elsevier.com/locate/aca

MnO_2 nanosheet-mediated ratiometric fluorescence biosensor for MicroRNA detection and imaging in living cells

Shuai Wang [a], Lei Wang [c], Xiaowen Xu [a], Xia Li [b], Wei Jiang [a, *]

[a] School of Chemistry and Chemical Engineering, Shandong University, 250100, Jinan, PR China
[b] Department of Chemistry, Liaocheng University, 252059, Liaocheng, PR China
[c] School of Pharmaceutical Sciences, Shandong University, 250012, Jinan, PR China

HIGHLIGHTS

- A ratiometric fluorescence biosensor was designed for miRNA detection.
- The strategy had been applied to differentiate miRNA expression levels in cells.
- The CHA displayed signal amplification ability, ensuring the sensitive detection.
- The strategy held great potential for the early clinical diagnostics.

GRAPHICAL ABSTRACT

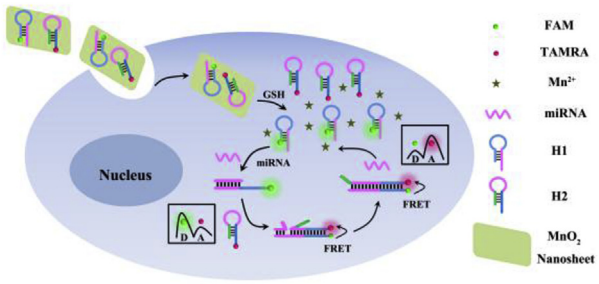

ARTICLE INFO

Article history:
Received 6 December 2018
Received in revised form
26 January 2019
Accepted 12 February 2019
Available online 4 March 2019

Keywords:
MnO_2 nanosheets
Ratiometric
MicroRNA detection
Cell imaging

ABSTRACT

MicroRNA (miRNA) plays significant roles in cell proliferation, differentiation and apoptosis, and has been considered to be valuable biomarker for cancer. Accurate and sensitive detection of miRNA is crucially significant for cancer diagnosis and treatment. Here, a MnO_2 nanosheet-mediated ratiometric fluorescence biosensor was designed for miRNA detection and imaging in living cells. It contained MnO_2 nanosheets acting as DNA carrier, and fluorescent donor (FAM)-labeled hairpin H1 (recognition probe) and fluorescent acceptor (TAMRA)-labeled hairpin H2 (amplification probe). When the biosensor entered cell by endocytosis, MnO_2 nanosheets were degraded to Mn^{2+} via intracellular glutathione (GSH) and the adsorbed hairpins H1 and H2 were released. The intracellular target miRNA-21 hybridized with the recognition unit of H1 to initiate catalyzed hairpin assembly (CHA) and a large amount of H1-H2 duplexes were produced. This brought fluorescent donor FAM and fluorescent acceptor TAMRA into close proximity to produce fluorescence resonance energy transfer (FRET), inducing a ratiometric fluorescent response (donor signal decreased and acceptor signal enhanced) for miRNA-21 detection. Furthermore, this method could be applied to differentiate the expression levels of miRNA-21 in HeLa, HepG-2 and L02 cells. These results indicated that the proposed method possessed great potential in the early diagnosis of miRNA-related diseases.

1. Introduction

MicroRNAs (miRNAs) are a group of noncoding RNA molecules existence in eukaryotic cells including plants and animals [1,2]. MiRNAs play significant roles in a variety of biological process, such

* Corresponding author.
E-mail address: wjiang@sdu.edu.cn (W. Jiang).

https://doi.org/10.1016/j.aca.2019.02.049
0003-2670/

as cell proliferation, differentiation and apoptosis by adjusting gene expression after transcription [3,4]. Accumulating evidences have demonstrated that the alterations of miRNA expression levels are closely related to the occurrence and development of cancers [5,6]. For instance, miRNA-21 was discovered to overexpress in various cancers, such as breast cancer, liver cancer and lung cancer [7–9]. Therefore, miRNA can be identified as a potential cancer biomarker [10,11]. The detection of miRNAs displays great significance for early cancer diagnosis. Nevertheless, due to the limitations of unique characteristics of miRNA, such as short size (approximately 22 nucleotides), low abundance, high sequence homology among family members and vulnerable degradability, miRNA detection method requires high sensitivity and accuracy [12].

Traditional miRNA detection strategies include Northern blotting, real-time quantitative polymerase chain reaction (qRT-PCR) and microarray [13–16]. Although these methods could achieve miRNAs detection in solutions or in cell lysates, they suffered from time-consuming steps, complex and expensive, impeding their wide applications. To overcome these issues, several new methods have been introduced for the detection of miRNAs, such as electrochemical methods [17–19], surface-enhanced Raman spectroscopy [20], colorimetric assays [21] and fluorescence methods [22,23]. Among them, fluorescence methods have received great attention because of short time consumption, great reproducibility, simple and high sensitivity [24,25]. Furthermore, fluorescence imaging can be applied to assay the target at the cellular level.

Currently,a series of methods for detecting miRNAs in living cells have been devised using fluorescence imaging techniques. Molecular beacon (MB) provided a method for monitoring miRNAs in living cells. It was designed to hybridize with the target sequence to generate fluorescent signal, achieving the detection of the target miRNA [26]. However, MB was delivered into cells by transfection, which exhibited low transfection efficiency, resulting in limited expression. In recently, nanomaterials, such as molybdenum disulfide (MoS_2), graphene oxide (GO) and gold nanoparticles (AuNPs), were widely used in biomedical and biosensing due to their unique optical properties and biocompatibility [27–29]. Moreover, a method using nanomaterial as a carrier has been increasingly applied for detection intracellular miRNAs. Wang research group designed an AuNPs loaded split-DNAzyme probe for imaging of miRNAs in cancer cells [30]. Kuang et al. developed a DNA driven core-satellite assembly probe based on AuNPs and quantum dots for detection of intracellular miRNAs [31]. Nevertheless, these measures are focused on single response signal and based on surveying the absolute variation in fluorescent intensity. These can prone to be affected by a variety of environmental factors, including nuclease degradation, thermodynamic fluctuations, uneven probe concentration distribution, cell autofluorescence and light source drift, impacting the accuracy of target detection [32].

Herein, a MnO_2 nanosheet-mediated ratiometric fluorescence biosensor was constructed for miRNA detection and imaging in living cells. MnO_2 nanosheet was a graphene-like sheet nanomaterial [33]. It could act as DNA nanocarrier to deliver FAM (donor) labeled recognition probes H1 and TAMRA (acceptor) labeled amplification probe H2 into cells. After entering the cell, MnO_2 nanosheets were degraded to Mn^{2+} by intracellular glutathione (GSH) [34] and hairpins H1 and H2 were released. In the presence of target miRNA-21, the catalyzed hairpin assembly (CHA) was triggered to form H1-H2 duplexes. This brought the fluorescent donor and fluorescent acceptor into close to each other to produce FRET, inducing ratiometric fluorescent response for miRNA-21 detection. Because of the self-correcting ability, the ratiometric biosensor utilized the changes of the emission intensity ratio of donor to acceptor to reduce the influence of experimental environmental. Furthermore, this method had been applied to differentiate the expression levels in HeLa, HepG-2 and L02 cells. These results indicated that the biosensor possessed great possible for the early diagnosis of miRNA-related diseases.

2. Experimental section

2.1. Chemicals and reagents

All of DNA oligonucleotides, miRNAs, DNase I endonuclease and Diethyl pyrocarbonate (DEPC) water were obtained from Sangon Biotech Co., Ltd. (Shanghai, China). DNA oligonucleotides and miRNAs sequences used in this assay were described in Table S1. Trihydroxymethyl aminomethane (Tris), manganese chloride tetrahydrate ($MnCl_2{\cdot}4H_2O$), hydrogen peroxide (H_2O_2), GSH and tetramethylammonium hydroxide (TMA·OH) were obtained from Macklin Biochemical Co., Ltd. (Shanghai, China). Antibiotics penicillin/streptomycin, cell culture medium, fetal bovine serum and PBS (pH 7.4) were purchased from Biological Industries (Beit-Haemek, Israel). The HeLa, HepG-2 and L02 cells were obtained from Procell Life Science & Technology Co., Ltd. (Wuhan, China). All chemicals were used as received without further purification. DEPC-treated deionized water was used throughout all the experiments.

2.2. Instruments

The fluorescence emission spectra were obtained on a Hitachi F-7000 fluorescence spectrophotometer (Hitachi, Japan). The ultraviolet-visible (UV-vis) absorption spectra were performed by a U-2910 spectrophotometer (Hitachi, Japan). Transmission electron microscopy (TEM) survey was recorded on a JEM-1011 transmission electron microscope (JEOL, Japan). The Raman spectrum was performed by a LabRAM HR800 spectrometer (Horiba Jobin Yvon, France). Fluorescence images were obtained with an Axio Observer 3 inverted fluorescence microscope (Carl Zeiss, Germany) with an objective lens of 63×. The MTT experiments were measured on a microplate reader (Tecan Austria GmbH, Austria). Dynamic light scattering (DLS) and zeta potential analysis were obtained on a ZetaSizer Nano ZS90 (Malvern Instrument, Worcs, UK). It was performed three times and each measurement consisted of 20 runs of 10 s.

2.3. Synthesis of MnO_2 nanosheets

The synthesized of MnO_2 nanosheets were based on the reported literature previously [35]. In a typical synthesis procedure, 20 mL mixture including 3 wt% H_2O_2 and 0.6 M TMA·OH was mixed with 10 mL $MnCl_2{\cdot}4H_2O$ (0.3 M) solution under stirring within 15 s. The obtaining dark brown solution was stirred at room temperature overnight and then collected via centrifugation at 10000 rpm for 10 min. The obtained crude product was washed several times with water and methanol and dried at 60 °C for 12 h to removal of residual solvent. In order to obtained MnO_2 nanosheets, 5 mg MnO_2 solid was dispersed in 10 mL water under ultrasonication for 10 h, and centrifuged to take the supernatant for the experiment.

2.4. In vitro fluorescence ratio detection of miRNA-21

Firstly, the oligonucleotides (H1 and H2) were heated to 95 °C for 5 min and then naturally cooled to room temperature. Subsequently, MnO_2 nanosheets (40 μg mL^{-1}) were mixed with H1 (20 nM) and H2 (120 nM) in Tris-HCl buffer (0.1 M Tris, 0.01 M NaCl, pH 7.4) and then added GSH (1 mM). Finally, the target miRNA-21 was added, followed by incubating at 37 °C for 40 min to trigger CHA.

2.5. Polyacrylamide gel electrophoresis experiment

The products of CHA reaction were analyzed by 15% non-denaturating polyacrylamide gel electrophoresis (PAGE) in 1 × electrophoresis Tris-borate-EDTA (TBE) buffer. The gel was stained with SYBR gold for 40 min and then imaging of gel was visualized by UV imaging system (Bio-RAD Laboratories Inc., USA).

2.6. Cell culture

L02 cells were fostered in DMEM medium supplemented with 10% fetal bovine serum and 1% antibiotics penicillin/streptomycin. HepG-2 cells were grown in MEM medium containing 10% fetal bovine serum and 1% antibiotics penicillin/streptomycin. HeLa cells were grown in 1640 medium supplemented with 10% fetal bovine serum and 1% antibiotics penicillin/streptomycin. All cells were incubated in a humidified atmosphere containing 5% CO_2 and 95% air at 37 °C.

2.7. MTT assay

MTT assay was utilized to detect the cytotoxicity of MnO_2 nanosheets. Firstly, HepG-2 cells were dispersed in a 96-well plate (5000 cells per well) and then incubated at 37 °C overnight. Then discard the original medium and added fresh cell medium containing different concentrations of MnO_2 nanosheets (0, 10, 20, 30, 40, 50, 60 and 70 μg mL^{-1}) and incubated for another 24 h. Next, 5 mg mL^{-1} MTT solutions (20 μL) were added and incubated for another 4 h. Finally, DMSO (100 μL) was mixed to per well to dissolve crystals. After 4 min of shock, the absorbance was surveyed at 490 nm by a microplate reader.

2.8. Fluorescence imaging

L02, HeLa and HepG-2 cells were first dispersed in chamber slides and incubated with 5% CO_2 and 95% air at 37 °C overnight. Then, the MnO_2 nanosheets and hairpin DNAs of H1 and H2, which were dispersed in cell culture medium, were added into cells and incubated another 4 h at 37 °C. Finally, washing cells three times with PBS buffer, the fluorescence imaging was performed using fluorescence microscope.

3. Results and discussion

3.1. Principle of miRNA detection and design

The principle of MnO_2 nanosheet-mediated ratiometric fluorescence biosensor was illustrated in Scheme 1. It contained MnO_2 nanosheets and two hairpins H1 and H2. MnO_2 nanosheets could absorb H1 and H2 as DNA nanocarrier and could act as fluorescent quencher. Hairpin H1 contained fluorescent donor (FAM) and recognition unit of target miRNA-21. Hairpin H2 contained fluorescent acceptor (TAMRA) and amplification unit. The spontaneous self-assembly between H1 and H2 were blocked due to the complementary sequences were inserted in the stems [36,37]. After being transferred to cells, MnO_2 nanosheets were degraded to Mn^{2+} by intracellular GSH and hairpin H1 and H2 were released. The intracellular target miRNA-21 hybridized with the recognition unit of H1. This could initiate the exposure of the hidden toehold in the stem of H1 to recognize H2, which could substitute the miRNA-21 from H1 to form steady H1-H2 double-stranded structure. During the CHA process, fluorescent donor in the 3' terminal of H1 was approach to the acceptor (located at H2) to generate FRET, producing a ratiometric fluorescent response (donor signal decreased and acceptor signal enhanced) for miRNA-21 detection. Furthermore, the released target miRNA-21 could trigger the next CHA to generate a great deal of H1-H2 complexes, resulting in signal magnification. In this manner, the detection and intracellular imaging of miRNA-21 could be achieved.

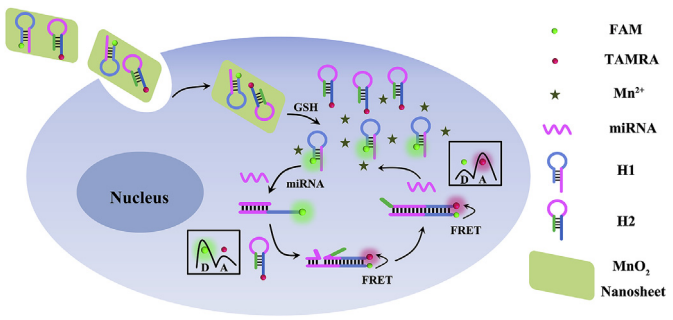

Scheme 1. Scheme illustration of MnO_2 nanosheet-mediated ratiometric fluorescence biosensor for miRNA detection and imaging.

3.2. Synthesis and characterization of MnO_2 nanosheets

The synthesized of MnO_2 nanosheets were by utilizing H_2O_2 to oxidize $MnCl_2 \cdot 4H_2O$ in the presence of TMA·OH and characterized by the TEM, UV-vis spectroscopy, DLS and Raman spectra. As shown in Fig. 1, the synthesized product exhibited a lamellar structure with a transverse diameter range of 100–350 nm and a strong UV absorption peak centered at 360 nm. In the Raman spectra, two major vibrational features corresponding to MnO_2 could be identified at 570 and 640 cm^{-1}. The Raman band at 570 cm^{-1} was due to the Mn-O stretching vibration, while the band located at 640 cm^{-1} could be attributed to the Mn-O symmetric stretching vibration [38,39]. In addition, zeta potential analysis displayed that it had a negative charge (−9.21 mV). These results indicated that the experiment successfully synthesized MnO_2 nanosheets.

Next, we performed absorption and DLS characterization of hairpin-assembled MnO_2 nanosheets. As depicted in Fig. S1, hairpin-assembled MnO_2 nanosheets exhibited a strong UV absorption peak centered at 260, 360 and 560 nm. The absorption peak at 360 nm was the characteristic peak of MnO_2 nanosheet, while the peak located at 260 nm and 560 nm could be attributed to the dye-labeled hairpin probe H1 and H2. At the same time, compared to the individual nanosheets (100–350 nm), we could discover that the transverse diameter of hairpin-assembled MnO_2 nanosheets increases (220–950 nm). These results indicated that hairpin probe H1 and H2 could be adsorbed onto the MnO_2 nanosheets.

In addition, we tested the fluorescence quenching ability of MnO_2 nanosheets for fluorescent dyes (FAM and TAMRA) by fluorescence analysis. As shown in Fig. S2A, H1 (labeled FAM) displayed strong fluorescence emission around 520 nm. However, the fluorescence intensities of H1 solutions would be gradually reduce with the MnO_2 nanosheets concentrations increased until completely quenched at the concentration of 40 μg mL^{-1}. Similar conclusion was also obtained utilizing TAMRA-labeled probe H2 (Fig. S2B). These results showed that MnO_2 nanosheets could effectively quench the fluorescence of dyes. In addition, when GSH was present in solution, the fluorescences of H1 and H2 were recovered gradually by degrees because MnO_2 nanosheets could be degraded and released hairpin probes (Fig. S3).

3.3. Fluorescence ratio detection in vitro

We examined the practicability of the MnO_2 nanosheet-

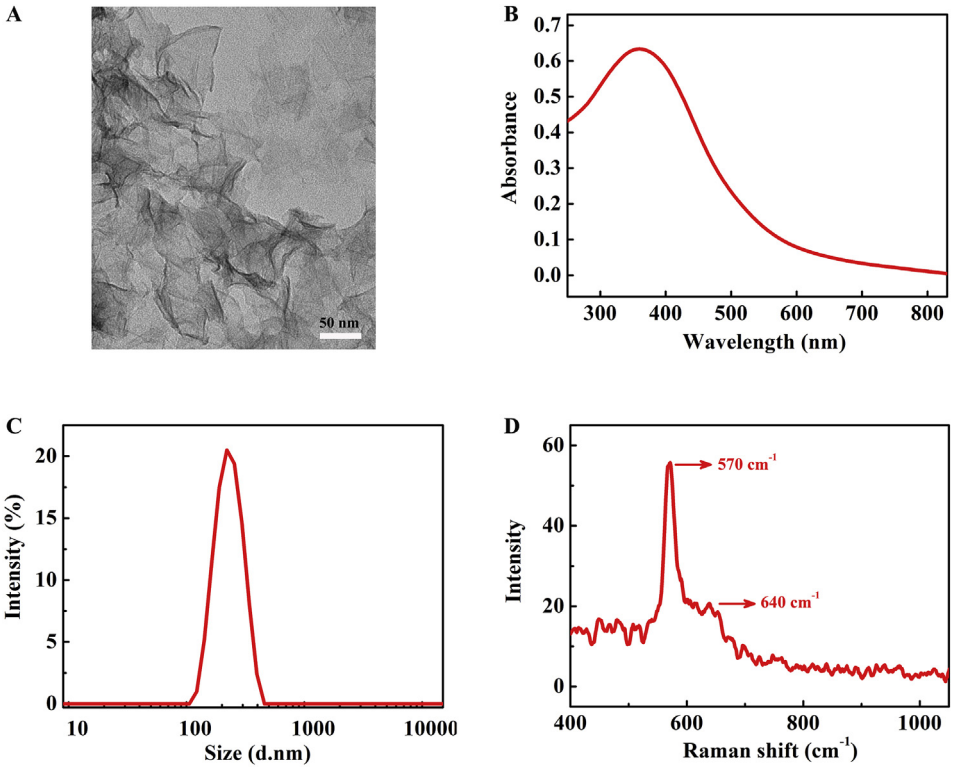

Fig. 1. Characterization of MnO_2 nanosheets. (A) TEM images, (B) UV-vis absorption spectrum, (C) DLS and (D) Raman spectrum results.

mediated ratiometric fluorescence biosensor for miRNA detection in vitro. As depicted in Fig. 2A, we noticed that the fluorescence of H1 (520 nm) was strong (black curve) and H2 exhibited a weak fluorescence emission peak at 570 nm (purple curve). It could be attributed to the abruption of the FRET pair. Compared to absence of target (red curve), the fluorescence emission peak of H1 was weakened and the signal of H2 was enhancement at 570 nm with the addition of miRNA-21 (blue curve). The reason was that the donor and acceptor were approach to each other, resulting that the energy was transferred from the donor to acceptor. The ratio of fluorescence intensities of $(F_A/F_D)_{positive}$ and $(F_A/F_D)_{negative}$, which respectively represented the fluorescence of the acceptor to donor ratio in the presence and the absence of miRNA-21, could be utilized as an output signal. To further confirm the feasibility of the detection of miRNA, the CHA reaction sequences and the products were analyzed by using PAGE. As displayed in Fig. 2B, the bands in lanes 1, 2 and 3 correspond to miRNA-21, H1 and H2, respectively. The H1 and H2 alone were mixed without the addition of miRNA-21, and no obvious H1-H2 duplex band (lane 4) was observed, demonstrating that the hairpin H1 and hairpin H2 could coexist in solutions and no CHA occurred. In the presence of miRNA-21, a strong band that migrated rather slowly (lane 5) was observed, suggesting that the CHA had taken `place and the self-assembled complex of two hairpins was formed. These results demonstrated that this method could be adopted for miRNA-21 detection.

3.4. Optimization of experimental conditions

To acquire the best assay capability, the reaction conditions, such as the ratio of H1 and H2 and reaction time were investigated

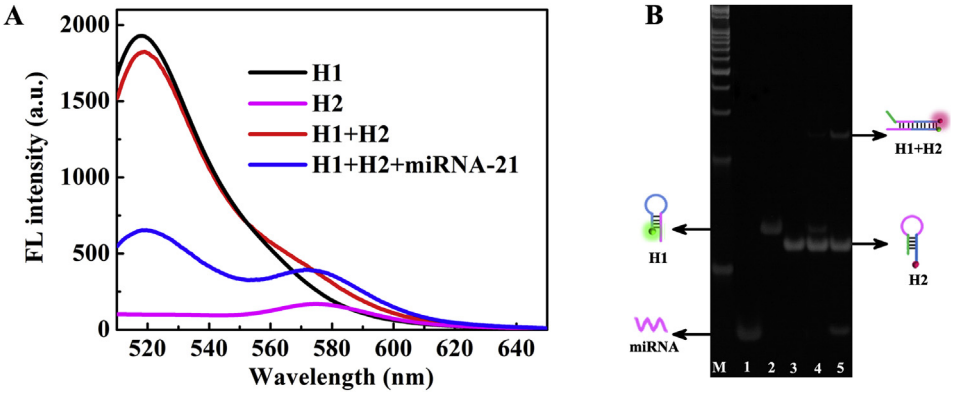

Fig. 2. (A) FRET detection of different systems: black curve, H1; purple curve, H2; red curve, H1+H2; blue curve,H1+H2+miRNA-21. All systems were excited at 488 nm. (B) PAGE demonstration of CHA reaction: lane M, DNA marker; lane 1, miRNA-21; lane 2, H1; lane 3, H2; lane 4, H1+H2; lane 5, H1+H2+miRNA-21. (For interpretation of the references to color in this figure legend, the reader is referred to the Web version of this article.)

in this article (Fig. S4). The optimal ratio of H1 and H2 was 1:6 and the reactions could complete within 40 min.

3.5. Stability experiment

To investigate the stability of this biosensor, we calculated the relative standard deviation (RSD) of intra- and interassay (n = 3). The RSD obtained from the intraday precision were 3.8%, 2.0% and 1.2% at the miRNA-21 concentrations of 5.0×10^{-9} mol L^{-1}, 1.0×10^{-8} mol L^{-1} and 1.5×10^{-8} mol L^{-1}, respectively. The RSD of interday precision were 4.3%, 3.8% and 1.9% at same miRNA-21 concentrations in three days. These results indicated that this sensor displayed a good stability.

In addition, we compared the effect of nuclease Dnase I (cleave ssDNA and dsDNA) toward ratiometric fluorescence probes and single dye fluorescence probe (Fig. S5). When Dnase I was mixed with ratiometric fluorescence probes H1 and H2, the ratio of F_A/F_D hardly changes (F_A and F_D respectively represented the fluorescence intensity of the acceptor and donor), suggesting that no false positive signal was generated. However, when added Dnase I into single dye fluorescent probe, gradually enhanced fluorescence signal was observed that would be undistinguishable from a true target miRNA-21 binding response. Effectively, both types of probes could be destroyed by Dnase I. The difference was that the signal would change after the single dye probe was destroyed while the ratiometric probe would not because the donor and acceptor were not brought to each other. The results certified that the ratiometric probe could effectively avoid the generation of false positive signals and improve the accuracy of miRNA detection.

3.6. Sensitivity

Under the optimized conditions discussed above, the analytical capability of the sensing system were recorded in vitro by measuring the ratio of $(F_A/F_D)_{positive}/(F_A/F_D)_{negative}$ upon the addition of miRNA-21 at different amounts. As depicted in Fig. 3, the ratio of the fluorescence intensities of $(F_A/F_D)_{positive}/(F_A/F_D)_{negative}$ enhanced linearly with the concentration range from 0.1 to 20 nM and the linear equation was $(F_A/F_D)_{positive}/(F_A/F_D)_{negative} = 0.2352C + 1.0001$ (C represented the concentration of miRNA-21; R = 0.9974). The limits of detection (LOD) of miRNA-21 was estimated (3σ/K, σ was the standard deviation of the blank solution) to be 73 pM. It was lower than most of the reported method and the advantage of ratiometric biosensor compared with some already reported strategies were exhibited in Table S2. This result indicated that ratiometric fluorescence biosensor could achieve sensitive detection of miRNA-21.

3.7. Selectivity

Sequence similarity between family members was a significant feature of miRNA, and a great challenge for intracellular miRNA detection was to discriminate differences between members of miRNA family. To further verify the specificity of the sensing system, we compared the ratio of $(F_A/F_D)_{positive}/(F_A/F_D)_{negative}$ responses to miRNA-21 and four interfering miRNAs, including miRNA-141, let-7a, let-7b and miRNA-21-5p. As shown in Fig. 4, the ratio of $(F_A/F_D)_{positive}/(F_A/F_D)_{negative}$ of interfering miRNAs were all close to the 1, and obviously lower than that from miRNA-21 the same concentration. The degrees of interference (DI) value for these interfering miRNAs were calculated according to the following equation:

$$DI = \frac{A - C}{B - C} \times 100\%$$

where A was the $(F_A/F_D)_{positive}$ of interfering miRNAs, B was the $(F_A/F_D)_{positive}$ of miRNA-21 and C was the $(F_A/F_D)_{negative}$ (blank). The DI values for the four interfering miRNAs were 0.1%, 1.3%, 0.2% and 0.3%, respectively. These results suggesting that the proposed sensor exhibited a high selectivity for miRNA detection.

3.8. MiRNA-21 imaging in living cells

Cytotoxicity was a key factor to consider in the design of intracellular nanoprobe systems. The cytotoxicity of MnO_2 nanosheets was first investigated by MTT assay. HepG-2 cells were incubated separately with different concentrations of MnO_2

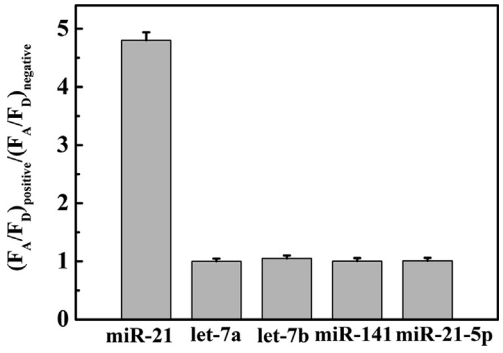

Fig. 4. Specificity of this developed strategy toward miRNA-21. $(F_A/F_D)_{positive}$ and $(F_A/F_D)_{negative}$ represented the proportion of fluorescence of the acceptor to donor in the presence and the absence of miRNA-21, respectively.

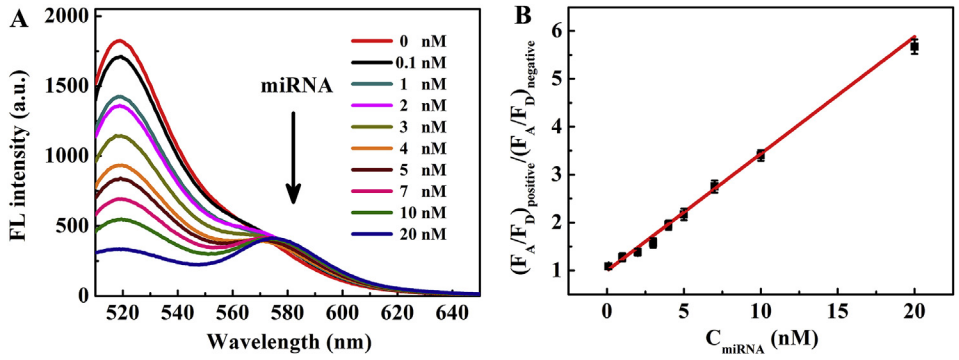

Fig. 3. (A) Fluorescence emission spectra of different concentrations (0, 0.1 nM, 1 nM, 2 nM, 3 nM, 4 nM, 5 nM, 7 nM, 10 nM and 20 nM) of miRNA-21. (B) Changes of the value of $(F_A/F_D)_{positive}/(F_A/F_D)_{negative}$ with miRNA-21 concentration. $(F_A/F_D)_{positive}$ and $(F_A/F_D)_{negative}$ represented the proportion of fluorescence of the acceptor to donor in the presence and the absence of miRNA-21, respectively.

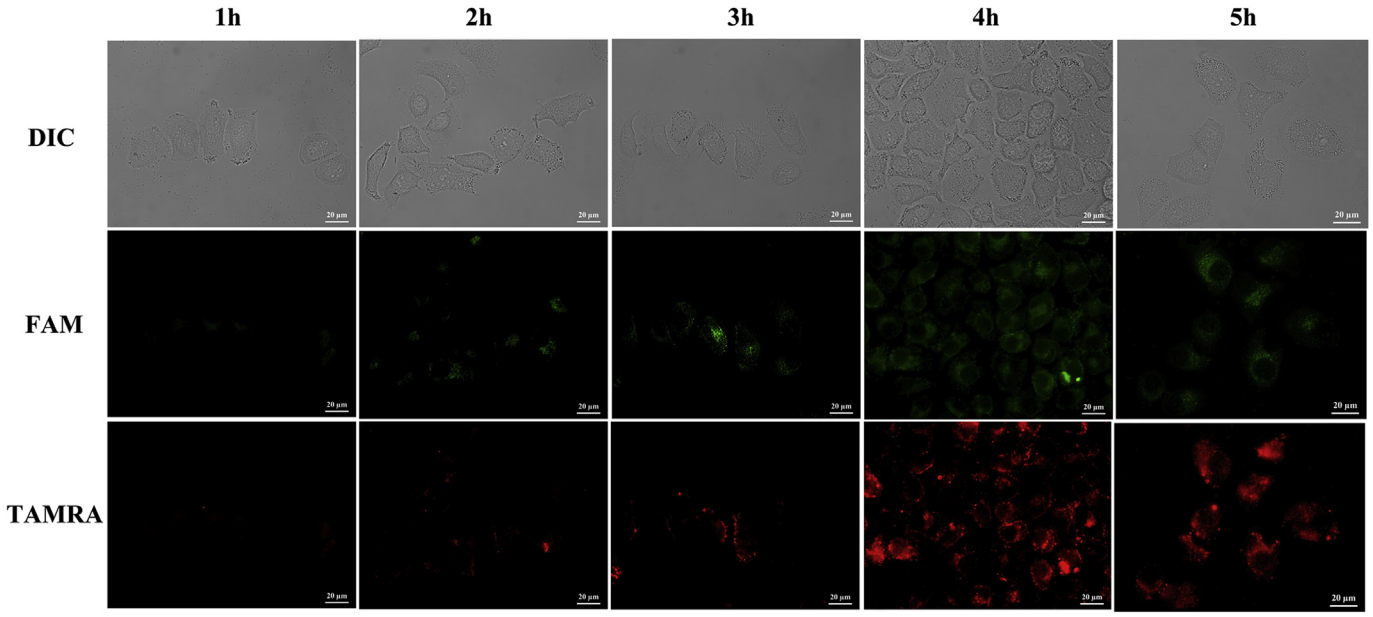

Fig. 5. Fluorescence imaging of intracellular miRNA-21 in HepG-2 cells under different incubation times from 1 to 5 h. Scale bar is 20 μm.

nanosheets for 24 h. As depicted in Fig. S6, when MnO_2 nanosheets concentration attained 70 μg mL^{-1}, the cell viability was still above 83%. This result displayed that MnO_2 nanosheets possessed low cytotoxicity to HepG-2 cells. Next, HepG-2 cells were incubated with the MnO_2 nanosheets and hairpin DNAs for different times (1–5 h) to optimize incubation time between probe and cell. As showed in Fig. 5, as the incubation time prolonged, the red fluorescent in HepG-2 cells tend to increased gradually until saturation reached at 4 h. The fluorescence intensity did not increase with further increase of incubation time. This result indicated that increasing FRET signal could be obtained after incubation 4 h and this biosensor could be applied to miRNAs imaging.

Finally, we explored the performance of the biosensor to the imaging of miRNA-21 in living cells. Cancer cells HeLa and HepG-2, which overexpressed miRNA-21, were choose as the positive cell and L02 (normal cell) with minimal level of miRNA-21 as control cell [40]. As shown in Fig. 6, after incubation with the ratio probe for 4 h, HeLa cells and HepG-2 cells exhibited weakly green fluorescent

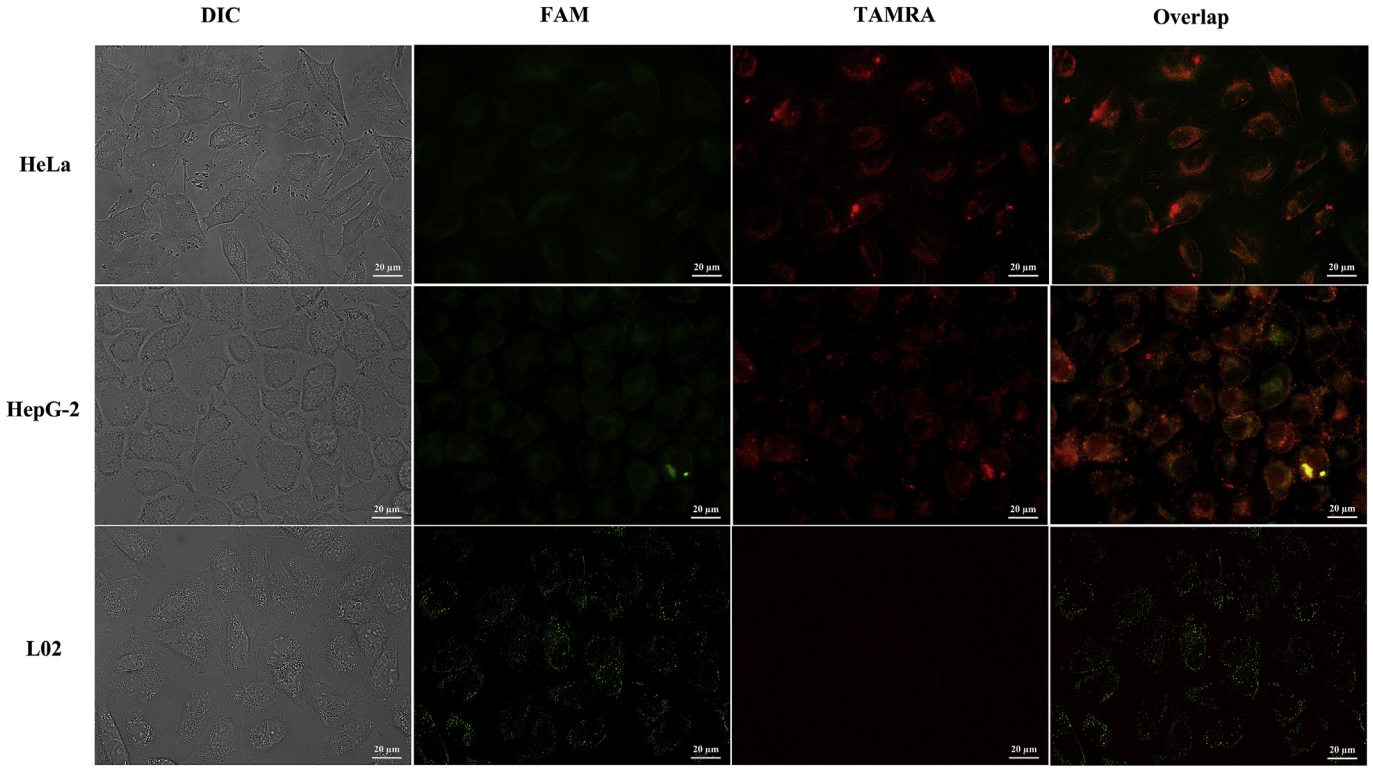

Fig. 6. Fluorescence imaging of miRNA-21 in HeLa cells, HepG-2 cells and L02 cells. Scale bar is 20 μm.

signals (FAM) and obvious red fluorescent signals (TAMRA), demonstrating that HeLa and HepG-2 displayed the higher level of expression of miRNA-21. However, L02 cells displayed strong green fluorescence and insignificant red fluorescence, suggesting that L02 cells possessed a relatively low miRNA-21 expression level. These results were consistent with conventional technique qRT-PCR (Fig. S7) and previously reported intracellular expression levels of miRNA-21 [30]. These experimental results demonstrated that the proposed ratiometric imaging method could distinguish normal cells and cancer cells, displaying potential application value in cancer diagnosis.

4. Conclusion

In summary,a MnO_2 nanosheet-mediated ratiometric fluorescence biosensor had been established for miRNA detection and imaging in living cells. Compared to the single dye detection, the ratiometric fluorescent method allowed fluorescence intensity to be simultaneously measured at two distinctly different wavelengths. It avoided the generation of false positive signals caused by experiment environment, such as enzymatic degradation, thermodynamic fluctuations, uneven probe concentration distribution and light source drift. The CHA signal amplification ensured that it exhibited a high sensitivity. Furthermore, the biosensor could be applied to differentiate the miRNA-21 expression levels in HeLa, HepG-2 and L02 cells. These results indicated that the biosensor possessed great possible for the early diagnosis of miRNA-related diseases.

Acknowledgements

This work was supported by the National Natural Science Foundation of China (Nos. 21475077, 21675100, 21675101 and 21705094).

Appendix A. Supplementary data

Supplementary data to this article can be found online at https://doi.org/10.1016/j.aca.2019.02.049.

References

[1] V. Ambros, The functions of animal microRNAs, Nature 432 (2004) 350–355.
[2] D.P. Bartel, MicroRNAs: genomics, biogenesis, mechanism, and function, Cell 116 (2004) 281–297.
[3] C.M. Croce, Causes and consequences of microRNA dysregulation in cancer, Nat. Rev. Genet. 10 (2009) 704–714.
[4] J.J. Rossi, New hope for a microRNA therapy for liver cancer, Cell 137 (2009) 990–992.
[5] H. Grosshans, W. Filipowicz, Molecular biology: the expanding world of small RNAs, Nature 451 (2008) 414–416.
[6] J.V. Tricoli, J.W. Jacobson, MicroRNA: potential for cancer detection, diagnosis, and prognosis, Cancer Res. 67 (2007) 4553–4555.
[7] L.B. Frankel, N.R. Christoffersen, A. Jacobsen, M. Lindow, A. Krogh, A.H. Lund, Programmed cell death 4 (PDCD4) is an important functional target of the microRNA miR-21 in breast cancer cells, J. Biol. Chem. 283 (2008) 1026–1033.
[8] J. Liu, S.K. Lau, V.A. Varma, R.A. Moffitt, M. Caldwell, T. Liu, A.N. Young, J.A. Petros, A.O. Osunkoya, T. Krogstad, B. Leyland-Jones, M.D. Wang, S. Nie, Molecular mapping of tumor heterogeneity on clinical tissue specimens with multiplexed quantum dots, ACS Nano 4 (2010) 2755–2765.
[9] Z.X. Wang, H.B. Bian, J.R. Wang, Z.X. Cheng, K.M. Wang, W. De, Prognostic significance of serum miRNA-21 expression in human non-small cell lung cancer, J. Surg. Oncol. 104 (2011) 847–851.
[10] M.A. Cortez, C. Bueso-Ramos, J. Ferdin, G. Lopez-Berestein, A.K. Sood, G.A. Calin, MicroRNAs in body fluids-the mix of hormones and biomarkers, Nat. Rev. Clin. Oncol. 8 (2011) 467–477.
[11] M.V. Iorio, P. Casalini, E. Tagliabue, S. Menard, C.M. Croce, MicroRNA profiling as a tool to understand prognosis, therapy response and resistance in breast cancer, Eur. J. Cancer 44 (2008) 2753–2759.
[12] L. He, G.J. Hannon, MicroRNAs: small RNAs with a big role in gene regulation, Nat. Rev. Genet. 5 (2004) 522–531.
[13] M. Lagos-Quintana, R. Rauhut, W. Lendeckel, T. Tuschl, Identification of novel genes coding for small expressed RNAs, Science 294 (2001) 853–858.
[14] P.T. Nelson, D.A. Baldwin, L.M. Scearce, J.C. Oberholtzer, J.W. Tobias, Z. Mourelatos, Microarray-based, high-throughput gene expression profiling of microRNAs, Nat. Methods 1 (2004) 155–161.
[15] C.C. Pritchard, H.H. Cheng, M. Tewari, MicroRNA profiling: approaches and considerations, Nat. Rev. Genet. 13 (2012) 358–369.
[16] C.K. Raymond, B.S. Roberts, P. Garrett-Engele, L.P. Lim, J.M. Johnson, Simple, quantitative primer-extension PCR assay for direct monitoring of microRNAs and short-interfering RNAs, RNA 11 (2005) 1737–1744.
[17] A. Chen, G.F. Gui, Y. Zhuo, Y.Q. Chai, Y. Xiang, R. Yuan, Signal-off electrochemiluminescence biosensor based on phi29 DNA polymerase mediated strand displacement amplification for microRNA detection, Anal. Chem. 87 (2015) 6328–6334.
[18] H.F. Dong, S. Jin, H.X. Ju, K.H. Hao, L.P. Xu, H.T. Lu, X.J. Zhang, Trace and label-free microRNA detection using oligonucleotide encapsulated silver nanoclusters as probes, Anal. Chem. 84 (2012) 8670–8674.
[19] T. Hou, W. Li, X.J. Liu, F. Li, Label-free and enzyme-free homogeneous electrochemical biosensing strategy based on hybridization chain reaction: a facile, sensitive, and highly specific microRNA assay, Anal. Chem. 87 (2015) 11368–11374.
[20] Y. He, X. Yang, R. Yuan, Y.Q. Chai, "Off" to "On" surface-enhanced Raman spectroscopy platform with padlock probe-based exponential rolling circle amplification for ultrasensitive detection of microRNA 155, Anal. Chem. 89 (2017) 2866–2872.
[21] J. Park, J.S. Yeo, Colorimetric detection of microRNA miR-21 based on nanoplasmonic core-satellite assembly, Chem. Commun. 50 (2014) 1366–1368.
[22] H.Y. Liu, T. Tian, Y.H. Zhang, L.H. Ding, J.H. Yu, M. Yan, Sensitive and rapid detection of microRNAs using hairpin probes-mediated exponential isothermal amplification, Biosens. Bioelectron. 89 (2017) 710–714.
[23] Y.J. Yang, J. Huang, X.H. Yang, X.X. He, K. Quan, N.L. Xie, M. Ou, K.M. Wang, Gold nanoparticle based hairpin-locked-DNAzyme probe for amplified miRNA imaging in living cells, Anal. Chem. 89 (2017) 5850–5856.
[24] R. Liao, K. He, C.Y. Chen, X.M. Chen, C.Q. Cai, Double-strand displacement biosensor and quencher-free fluorescence strategy for rapid detection of microRNA, Anal. Chem. 88 (2016) 4254–4258.
[25] Q. Zhang, F. Chen, F. Xu, Y.X. Zhao, C.H. Fan, Target-triggered three-way junction structure and polymerase/nicking enzyme synergetic isothermal quadratic DNA machine for highly specific, one-step, and rapid microRNA detection at attomolar level, Anal. Chem. 86 (2014) 8098–8105.
[26] Q. Yao, A.M. Zhang, H. Ma, S. Lin, X.X. Wang, J.G. Sun, Z.T. Chen, Novel molecular beacons to monitor microRNAs in non-small-cell lung cancer, Mol. Cell. Probes 26 (2012) 182–187.
[27] D.K. Ji, Y. Zhang, Y. Zang, J. Li, G.R. Chen, X.P. He, H. Tian, Targeted intracellular production of reactive oxygen species by a 2D molybdenum disulfide glycosheet, Adv. Mater. 28 (2016) 9356–9363.
[28] Y.H. Ma, W.T. Dou, Y.F. Pan, L.W. Dong, Y.X. Tan, X.P. He, H. Tian, H.Y. Wang, Fluorogenic 2D peptidosheet unravels CD47 as a potential biomarker for profiling hepatocellular carcinoma and cholangiocarcinoma tissues, Adv. Mater. 29 (2017), 1604253.
[29] X.P. He, X.L. Hu, T.D. James, J. Yoon, H. Tian, Multiplexed photoluminescent sensors: towards improved disease diagnostics, Chem. Soc. Rev. 46 (2017) 6687–6696.
[30] Y.N. Wu, J. Huang, X.H. Yang, Y.J. Yang, K. Quan, N.L. Xie, J. Li, C.B. Ma, K.M. Wang, Gold nanoparticle loaded split-DNAzyme probe for amplified miRNA detection in living cells, Anal. Chem. 89 (2017) 8377–8383.
[31] X.L. Zhao, L.G. Xu, M.Z. Sun, W. Ma, X.L. Wu, H. Kuang, L.B. Wang, C.L. Xu, Gold-quantum dot core-satellite assemblies for lighting up microRNA in vitro and in vivo, Small 12 (2016) 4662–4668.
[32] N.L. Rosi, D.A. Giljohann, C.S. Thaxton, A.K. Lytton-Jean, M.S. Han, C.A. Mirkin, Oligonucleotide-modified gold nanoparticles for intracellular gene regulation, Science 312 (2006) 1027–1030.
[33] D.G. He, X.X. He, K.M. Wang, X. Yang, X.X. Yang, X.C. Li, Z. Zou, Nanometer-sized manganese oxide-quenched fluorescent oligonucleotides: an effective sensing platform for probing biomolecular interactions, Chem. Commun. 50 (2014) 11049–11052.
[34] D.G. He, X.X. Yang, X.X. He, K.M. Wang, X. Yang, X. He, Z. Zou, A sensitive turn-on fluorescent probe for intracellular imaging of glutathione using single-layer MnO_2 nanosheet-quenched fluorescent carbon quantum dots, Chem. Commun. 51 (2015) 14764–14767.
[35] K. Kai, Y. Yoshida, H. Kageyama, G. Saito, T. Ishigaki, Y. Furukawa, J. Kawamata, Room-temperature synthesis of manganese oxide monosheets, J. Am. Chem. Soc. 130 (2008) 15938–15943.
[36] J.Y. Dai, H.F. He, Z.J. Duan, C.S. Zhou, Y.Y. Long, B.Z. Zheng, J. Du, Y. Guo, D. Xiao, Target-triggered autonomous assembly of DNA polymer chains and its application in colorimetric nucleic acid detection, J. Mater. Chem. B. 4 (2016) 3191–3194.
[37] F. Li, H.Q. Zhang, Z.X. Wang, X.K. Li, X.F. Li, X.C. Le, Dynamic DNA assemblies mediated by binding-induced DNA strand displacement, J. Am. Chem. Soc. 135 (2013) 2443–2446.
[38] C. Julien, M. Massot, R. Baddour-Hadjean, S. Franger, S. Bach, J.P. Pereira-Ramos, Raman spectra of birnessite manganese dioxides, Solid State Ionics 159 (2008) 345–356.
[39] Y.K. Hsu, Y.C. Chen, Y.G. Lin, L.C. Chen, K.H. Chen, Reversible phase transformation of MnO_2 nanosheets in an electrochemical capacitor investigated by in situ Raman spectroscopy, Chem. Commun. 47 (2011) 1252–1254.
[40] Y.Y. Wang, Z.P. Yu, Z. Zhang, R. Ren, S.S. Zhang, Orderly nucleic acid aggregates by electrostatic self-assembly in single cells for miRNA detection and visualizing, Analyst 141 (2016) 2861–2864.